Transp Porous Med
DOI 10.1007/s11242-016-0761-4

Experimental and Analytical Investigation of Spontaneous Imbibition in Water-Wet Carbonates

Nayef Alyafei[1] · **Ali Al-Menhali**[1] · **Martin J. Blunt**[1]

Received: 29 July 2015 / Accepted: 23 August 2016

Abstract We perform co-current spontaneous imbibition ambient-condition experiments in three carbonates with a wide range of permeability under strongly water-wet conditions. We measure water saturation profiles as a function of distance and time in air-filled rocks with no initial water saturation using X-ray CT scanning. We demonstrate that the saturation profiles are functions of distance divided by the square root of time. We also demonstrate that the profiles are consistent with analytical solutions for imbibition in one dimension, and using reasonable estimates of relative permeability and capillary pressure, we can match the experimental results. We discuss how, in combination with conventional measurements of relative permeability (steady-state or using Buckley–Leverett theory in an unsteady-state experiment), the capillary pressure can be determined, or how the relative permeability can be determined from the spontaneous imbibition experiment and the capillary pressure.

Keywords Spontaneous imbibition · Analytical solution · Relative permeability · Capillary pressure · Capillary-dominated flow · Carbonates

List of Symbols

α	Capillary pressure exponent
λ_{nw}	Mobility of the non-wetting phase
λ_t	Total mobility
λ_w	Mobility of the wetting phase
ρ_{nw}	Density of the non-wetting phase
ρ_w	Density of the wetting phase
μ_{nw}	Viscosity of the non-wetting phase
μ_w	Viscosity of the wetting phase

✉ Nayef Alyafei
nayef.alyafei@qatar.tamu.edu

[1] Qatar Carbonates and Carbon Storage Research Centre, Department of Earth Science and Engineering, Imperial College, London SW7 2AZ, UK

Published online: 06 September 2016

ϕ	Porosity
ω	Imbibed distance over square root of time
C	Proportionality constant used in the analytical solution
$D(S_w$	Capillary dispersion coefficient
f	Fractional flow for viscous-dominated flow
f'	First derivative of f
F	Fractional flow for capillary-dominated flow
F'	First derivative of F
F''	Second derivative of F
g_x	Gravitational acceleration
k	Permeability
k_r	Relative permeability
k_{rg}	Gas relative permeability
$k_{rg,max}$	Maximum gas relative permeability
k_{rw}	Water relative permeability
$k_{rw,max}$	Maximum water relative permeability
m	Corey gas exponent
n	Corey water exponent
P_c	Capillary pressure
$P_{c,entry}$	Entry capillary pressure
P_{nw}	Non-wetting phase pressure
P_w	Wetting phase pressure
q_t	Total Darcy velocity
q_{nw}	Non-wetting phase Darcy velocity
q_w	Wetting phase Darcy velocity
S_{gr}	Residual gas saturation
S_w	Water saturation
S_{wi}	Initial water saturation
S_{wir}	Irreducible water saturation
t	Time
v_{sh}	Shockfront moving speed
v_{shD}	Dimensionless shockfront moving speed
x	Distance

1 Introduction

With over half of the world's conventional oil contained in fractured carbonate reservoirs, it is important that the fundamentals of fluid flow from fracture to matrix by spontaneous imbibition are understood. Spontaneous imbibition is one of the main recovery mechanisms in these reservoirs; in addition, it is also the process rendering the non-wetting phase, CO_2, immobile in CO_2 sequestration (Morrow and Mason 2001; Pentland et al. 2011). Spontaneous imbibition can occur in two different modes: co-current and counter-current. Co-current is when the oil (or gas) and brine flow in the same direction. Counter-current imbibition occurs when the two phases flow in opposite directions from the same inlet. In the reservoir, counter-current displacement will dominate if matrix blocks are completely surrounded by water; however, if the rock matrix blocks are not fully surrounded by water and if gravity segregation occurs, then co-current is the dominant flow (Bourbiaux and Kalaydjian 1990;

Pooladi-Dravish and Firoozabadi 2000; Unsal et al. 2007). The rate of water imbibition into the porous medium is a function of permeability, relative permeability, capillary pressure, initial water saturation, boundary conditions, viscosity, interfacial tension, and wettability (Zhang et al. 1996; Graue and Fernø 2011; Mason and Morrow 2013).

McWhorter and Sunada (1990, 1992) first proposed an analytical solution for spontaneous imbibition, where the displacement is controlled entirely by capillary forces. However, it was not appreciated until the work of Schmid et al. (2011) that it is indeed a closed-form solution and generally applicable for spontaneous imbibition. This solution is a useful complement to the Buckley–Leverett solution. It can be used in combination with experimental results to determine, or at least constrain, capillary pressure and relative permeability. In addition, it is useful for the analysis of recovery in fractured reservoirs.

In this paper, we show a simplified derivation of the Schmid et al. (2011) and Schmid and Geiger (2012) analytical solution for spontaneous imbibition. We then perform co-current spontaneous imbibition experiments using a medical CT for in situ monitoring of the saturation movement inside the rock samples. We combine the experiment with the analytical solution for spontaneous imbibition to estimate relative permeability and capillary pressure by matching these properties with the experimental saturation profile over the square root of time. Finally, we further discuss how to use the analytical solution to estimate relative permeability or capillary pressure.

1.1 Analytical Solution

Schmid et al. (2011) derived an analytical solution for spontaneous imbibition, where displacement is controlled entirely by capillary forces. We present the full derivation from the conservation equation to the exact solution, using a step-by-step simplified approach.

The analytical solution makes the following assumptions:

1. Incompressible fluids.
2. That the traditional multi-phase Darcy law is applicable for this process.
3. Gravitational forces are ignored.
4. There is no imposed viscous force, while viscous forces generated by the imbibition process are considered.
5. We assume that at the inlet the capillary pressure is zero with no capillary back pressure.
6. We will assume that the solutions are a function of the parameter $\omega = x/\sqrt{t}$; this is only valid at early time, before the imbibing water front has reached the far boundaries of the sample.

1.2 Equation Derivation

We start from the wetting phase conservation equation in one dimension for incompressible fluids:

$$\phi \frac{\partial S_{\mathrm{w}}}{\partial t} + \frac{\partial q_{\mathrm{w}}}{\partial x} = 0 \tag{1}$$

From the multiphase Darcy's law, the wetting phase Darcy velocity:

$$q_{\mathrm{w}} = -\frac{k k_{\mathrm{rw}}}{\mu_{\mathrm{w}}} \left(\frac{\partial P_{\mathrm{w}}}{\partial x} - \rho_{\mathrm{w}} g_x \right) \tag{2}$$

and the same for the non-wetting phase Darcy velocity:

$$q_{\mathrm{nw}} = -\frac{k k_{\mathrm{rnw}}}{\mu_{\mathrm{nw}}}\left(\frac{\partial P_{\mathrm{nw}}}{\partial x} - \rho_{\mathrm{nw}} g_x\right) \tag{3}$$

where $P_{\mathrm{c}} = P_{\mathrm{nw}} - P_{\mathrm{w}}$ is the capillary pressure and k_{r} is the relative permeability. k_{rnw}, k_{rw}, and P_{c} are functions of S_{w}. We define mobilities of the wetting phase and the non-wetting as:

$$\lambda_{\mathrm{w}} = \frac{k_{\mathrm{rw}}}{\mu_{\mathrm{w}}} \tag{4}$$

$$\lambda_{\mathrm{nw}} = \frac{k_{\mathrm{rnw}}}{\mu_{\mathrm{nw}}} \tag{5}$$

$$\lambda_{\mathrm{t}} = \lambda_{\mathrm{w}} + \lambda_{\mathrm{nw}} \tag{6}$$

Since $q_{\mathrm{t}} = q_{\mathrm{w}} + q_{\mathrm{nw}}$ is a constant in space for incompressible flow in one dimension, we can rewrite q_{w} as:

$$q_{\mathrm{w}} = \frac{\lambda_{\mathrm{w}}}{\lambda_{\mathrm{t}}}\left\{q_{\mathrm{t}} + k\lambda_{\mathrm{nw}}\left(\frac{\partial P_{\mathrm{c}}}{\partial x} + (\rho_{\mathrm{w}} - \rho_{\mathrm{nw}})g_x\right)\right\} \tag{7}$$

We eliminate the gravitational forces assuming that they are either small at the experimental (cm) scale or the displacement is horizontal. Then Eq. (7) becomes:

$$q_{\mathrm{w}} = f_{\mathrm{w}}(S_{\mathrm{w}})q_{\mathrm{t}} + \frac{k\lambda_{\mathrm{w}}\lambda_{\mathrm{nw}}}{\lambda_{\mathrm{t}}}\frac{\partial P_{\mathrm{c}}}{\partial x} \tag{8}$$

where f_{w} is the Buckley–Leverett fractional flow which is equal to $\lambda_{\mathrm{w}}/\lambda_{\mathrm{t}}$.

For counter-current imbibition, we set the total velocity (q_{t}) to zero which means that no fluid is injected and the movement of the wetting phase is matched by the volume of the non-wetting phase leaving the porous medium ($q_{\mathrm{nw}} = -q_{\mathrm{w}}$). Then Eq. (7) becomes:

$$q_{\mathrm{w}} = \frac{k\lambda_{\mathrm{w}}\lambda_{\mathrm{nw}}}{\lambda_{\mathrm{t}}}\frac{\partial P_{\mathrm{c}}}{\partial x} \tag{9}$$

For co-current imbibition instead we use Eq. (8) which we substitute into the wetting phase conservation equation, Eq. (1), to find:

$$\phi\frac{\partial S_{\mathrm{w}}}{\partial t} + \frac{\partial}{\partial x}\left(\frac{k\lambda_{\mathrm{w}}\lambda_{\mathrm{nw}}}{\lambda_{\mathrm{t}}}\frac{\partial P_{\mathrm{c}}}{\partial x}\right) + q_{\mathrm{t}}\frac{\partial f_{\mathrm{w}}}{\partial x} = 0 \tag{10}$$

We also substitute Eq. (9) for counter-current imbibition in the wetting phase conservation equation, Eq. (1),

$$\phi\frac{\mathrm{d}S_{\mathrm{w}}}{\mathrm{d}t} + \frac{\partial}{\partial x}\left(\frac{k\lambda_{\mathrm{w}}\lambda_{\mathrm{nw}}}{\lambda_{\mathrm{t}}}\frac{\partial P_{\mathrm{c}}}{\partial x}\right) = 0 \tag{11}$$

We can rewrite Eqs. (10) and (11) as nonlinear dispersion equations.

For co-current flow:

$$\phi\frac{\partial S_{\mathrm{w}}}{\partial t} = -q_{\mathrm{t}} f'_{\mathrm{w}}(S_{\mathrm{w}})\frac{\partial S_{\mathrm{w}}}{\partial x} + \frac{\partial}{\partial x}\left(D(S_{\mathrm{w}})\frac{\partial S_{\mathrm{w}}}{\partial x}\right) \tag{12}$$

and for counter-current flow:

$$\phi\frac{\partial S_{\mathrm{w}}}{\partial t} = \frac{\partial}{\partial x}\left(D(S_{\mathrm{w}})\frac{\partial S_{\mathrm{w}}}{\partial x}\right) \tag{13}$$

where $D(S_w)$ is the capillary dispersion coefficient:

$$D(S_w) = -\frac{k\lambda_w\lambda_{nw}}{\lambda_t}\frac{dP_c}{dS_w} \tag{14}$$

In the traditional Buckley–Leverett analysis (ignoring capillary forces), we find that the solution is a function of $v = x/t$ only, where the dimensionless wave speed is given by the saturation derivative of the fractional flow ($v_{shD} = df_w/dS_w$ where $v_{sh} = q_t/\phi\, v_D$) (Buckley and Leverett 1942; Dake 1983).

We propose an analogy here, but for capillary-controlled flow, which is dispersive: the imbibing front moves a distance x that instead of scaling with t, as in the Buckley–Leverett case, scales as $\sqrt{t}$ (Garg et al. 1996; Handy 1960; Babadagli and Ershaghi 1992; Li and Horne 2001; Olafuyi et al. 2007. Hence, we will now attempt to find a solution that can be written as a function of:

$$\omega = \frac{x}{\sqrt{t}} \tag{15}$$

We will show that this assumption is valid for our experiments. However, some experiments show a deviation from $\sqrt{t}$ behavior (Mason et al. 2010, 2012). Mason et al. (2012) reported that for n-decane and brine counter-current flow, the front movement scales approximately linearly with time, as the resistance to flow is controlled by the capillary back pressure, which is the pressure opposing the production of the non-wetting phase (Unsal et al. 2009; Haugen et al. 2014). The scaling we use is only valid under the assumptions mentioned at the beginning of the section, and specifically when the flow is entirely driven by capillary forces within the rock.

Then from analogy with the Buckley–Leverett analysis, we state that for some capillary fractional flow $F(1 \geq F \geq 0)$ and constant C:

$$\omega = \frac{2C}{\phi}F'(S_w) \tag{16}$$

Hence

$$\frac{d\omega}{dS_w} = \frac{2C}{\phi}F''(S_w) \tag{17}$$

The factor $2C/\phi$, where C is a constant, is introduced to make F dimensionless. The dimensions of C are length/$\sqrt{\text{time}}$ or m s$^{-1/2}$. Then we define the following derivatives:

$$\frac{\partial S_w}{\partial t} = \frac{dS_w}{d\omega}\frac{\partial\omega}{\partial t} = -\omega\frac{1}{2t}\frac{dS_w}{d\omega} \tag{18}$$

$$\frac{\partial S_w}{\partial x} = \frac{dS_w}{d\omega}\frac{\partial\omega}{\partial x} = \frac{1}{\sqrt{t}}\frac{dS_w}{d\omega} \tag{19}$$

With these derivations, we can rewrite Eq. (10) as an ordinary differential equation for co-current flow:

$$\omega\frac{dS_w}{d\omega} + 2\frac{d}{d\omega}\left(D(S_w)\frac{dS_w}{d\omega}\right) - 2Cf_w'(S_w)\frac{dS_w}{d\omega} = 0 \tag{20}$$

and rewrite Eq. (11) for counter-current flow:

$$\omega\frac{dS_w}{d\omega} + 2\frac{d}{d\omega}\left(D(S_w)\frac{dS_w}{d\omega}\right) = 0 \tag{21}$$

Then we integrate once, for co-current flow:

$$\int(\omega - f'(S_w))dS_w = -\frac{2D}{\phi}\frac{dS_w}{d\omega} \tag{22}$$

and for counter-current flow:

$$\int \omega \mathrm{d}S_{\mathrm{w}} = -\frac{2D}{\phi}\frac{\mathrm{d}S_{\mathrm{w}}}{\mathrm{d}\omega} \tag{23}$$

note that the integration constant is zero since we define $F(S_{\mathrm{wir}}) = 0$ and also $D(S_{\mathrm{wir}})$=0.

Then, we substitute $\omega = \frac{2C}{\phi}F'$ from Eq. (16) to evaluate the integrals on the left-hand side of Eqs.(22) and (23), and $\frac{\mathrm{d}\omega}{\mathrm{d}S_{\mathrm{w}}} = \frac{2C}{\phi}F''$ from Eq. (17). We obtain for co-current flow:

$$(F - f)F'' = -\frac{\phi}{2C^2}D \tag{24}$$

and for counter-current flow:

$$FF'' = -\frac{\phi}{2C^2}D \tag{25}$$

Formally this is an analytic solution to the equations, since they define F and hence the whole solution.

1.3 Solving the Equations

Schmid et al. (2011) presents a formal solution to Eq. 24 as

$$F = \int\int \frac{-\phi}{2C^2}\frac{D}{(F - f)}\mathrm{d}^2 S_{\mathrm{w}} \tag{26}$$

and similarly with $f = 0$ for counter-current flow.

Equation (26) is implicit in F and so can only be solved iteratively. Schmid et al. (2011) do this by first assuming a functional form for $F(F = S_{\mathrm{w}}$ is the first guess), solving Eq. (26) and finding a new $F(S_{\mathrm{w}})$, which is then placed in the integral again.

To evaluate F and the solution $S_{\mathrm{w}}(\omega)$, we do require an iterative method. We instead though develop a simple approach to finding the solution using a numerical method, giving:

$$F''(S_i) \approx \frac{F(S_{i+2}) - 2F(S_{i+1}) + F(S_i)}{\Delta S^2} \tag{27}$$

where S_i is the saturation evaluated at grid block i. We substitute Eq. (27) into Eq. (24) for co-current flow:

$$\left(\frac{F(S_{i+2}) + F(S_i) - 2F(S_{i+1})}{\Delta S^2}\right)(F(S_i) - f(S_i)) = -\frac{\phi}{2C^2}D(S_i) \tag{28}$$

similarly, we substitute Eq. (27) into Eq. (25) for counter-current flow:

$$\left(\frac{F(S_{i+2}) + F(S_i) - 2F(S_{i+1})}{\Delta S^2}\right)F(S_i) = -\frac{\phi}{2C^2}D(S_i) \tag{29}$$

Now, we multiply both sides by ΔS^2, for co-current flow:

$$(F(S_i) + F(S_{i+2}) - 2F(S_{i+1}))\,(F(S_i) - f(S_i)) = -\frac{\phi}{2C^2}D(S_i)\Delta S^2 \tag{30}$$

for counter-current flow:

$$(F(S_i) + F(S_{i+2}) - 2F(S_{i+1}))\,F(S_i) = -\frac{\phi}{2C^2}D(S_i)\Delta S^2 \tag{31}$$

Let us assume that $X = F(S_i)$, then Eq. (30) for co-current flow becomes:

$$X^2 + (F(S_{i+2}) - 2F(S_{i+1}) - f(S_i))X - F(S_{i+2})f(S_i) + 2F(S_{i+1})f(S_i) + \frac{\phi}{2C^2}D(S_i)\Delta S^2 = 0 \tag{32}$$

and for counter-current flow:

$$X^2 + (F(S_{i+2}) - 2F(S_{i+1}))X + \frac{\phi}{2C^2}D(S_i)\Delta S^2 = 0 \tag{33}$$

from the quadratic formula, the solution for $X = F(S_i)$ for co-current flow becomes:

$$F(S_i) = \Big(F(S_{i+1}) - 0.5F(S_{i+2}) + 0.5f(S_i)\Big) + \sqrt{\Big(F(S_{i+1}) - 0.5F(S_{i+2}) + 0.5f(S_i)\Big)^2 + F(S_{i+2})f(S_i) - 2F(S_{i+1})f(S_i) - \frac{\phi}{2C^2}D(S_i)\Delta S^2} \tag{34}$$

For counter-current flow:

$$F(S_i) = \Big(F(S_{i+1}) - 0.5F(S_{i+2})\Big) + \sqrt{\Big(F(S_{i+1}) - 0.5F(S_{i+2})\Big)^2 - \frac{\phi}{2C^2}D(S_i)\Delta S^2} \tag{35}$$

where the positive root gives physically valid solution. We calculate $F(S_w)$ with n gridblocks from S_{wir} to S^*. S^* represents the inlet conditions, defined such that $P_c(S^*) = 0$. At the inlet $F(S^*) = F(S_n) = 1$. We assume that the wave speed is zero, hence $F'(S^*) = 0$, or $F(S_{n-1}) = F(S_n) = 1$. This then allows us to use Eqs. (34) or (35) as appropriate to calculate $F(S_{n-2})$ and so on to $F(S_1)$ where $S_1 = S_{wir}$.

Then, once $F(S_i)$ and C are determined, $S_w(\omega)$ is found using Eq. (16), with $F'(S_i) = (F(S_{i+1}) - F(S_i))/\Delta S$. These equations have been coded into spreadsheets[1]. Iteration is involved, as we need to guess the value of C to satisfy the following condition:

$$F(S_{wir}) = F(S_{i=1}) = 0 \tag{36}$$

In addition, the integrated saturation curve must equal to the total volume imbibed:

$$\int_{S_{wir}}^{S_{w,max}} x(S_w, t)\mathrm{d}S_w = \frac{q_w(t)}{\phi} = \frac{2C\sqrt{t}}{\phi} \tag{37}$$

We start the process by guessing an initial value of C and we keep changing it until we satisfy Eq. (36). This can be done easily by hand to determine C to 3 or 4 significant figures in a few steps.

Note that the analytical solution is only valid for the early time of imbibition where the flow is entirely governed by capillary forces in the absence of constraining boundaries. The late time is governed by boundary/diffusion where the water front reaches the boundary and the recovery rate decays exponentially (Li and Horne 2001; Suzanne et al. 2003; Olafuyi et al. 2007).

[1] The spreadsheets can be downloaded from https://www.imperial.ac.uk/engineering/departments/earth-science/research/research-groups/perm/research/pore-scale-modelling/software/

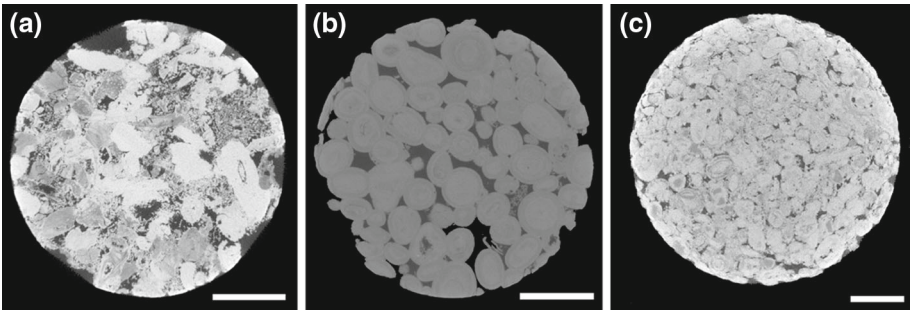

Fig. 1 Slices (two-dimensional sections) of three-dimensional X-ray micro-tomography images of **a** Estaillades, **b** Ketton, and **c** Portland. The *white bar* represents 1 mm

2 Experimental and Theoretical Methods

2.1 Rocks

We study three quarry rocks: Estaillades, Ketton, and Portland limestones. Estaillades limestone is from the Estaillade Formation, found in the Oppède quarry, south of France. It was deposited between 100 and 72 million years ago, corresponding to the Cenomanian and Campanian ages, and consists of 99 % calcite; the remaining 1 % accounts for traces of dolomite and silica (Wright et al. 1995). Ketton limestone is from the Lincolnshire Formation, located in Rutland, east Midlands, UK. It was deposited between 176 and 167 million years ago, corresponding to the Toarcian and Bajocian ages, and consists of of 99.1 % calcite and 0.9 % quartz (Ashton 1980). Portland limestone is from the Portland Formation, UK. It was deposited between 152 and 145 million years ago, corresponding to the Late Jurassic age, and consists of 96.6 % calcite and 3.4 % quartz (Brenchley and Rawson 2006). Figure 1 shows micro-CT images of the three rocks.

2.2 Fluids and Experimental Conditions

We conduct our experiments at ambient conditions of atmospheric pressure and room temperature of $20 \pm 1\,^{\circ}\mathrm{C}$. We use air as the non-wetting phase and brine, with 5 wt% sodium chloride (NaCl) and 1 wt% potassium chloride (KCl) mixed with deionized water, as the wetting liquid phase. Although air is compressible, the pressure change in the air phase during the experiment is assumed to be negligible, with little or no volume change. In addition, we equilibrate the brine with the carbonate samples for 48 h by mixing them using magnetic stirrer to eliminate any reaction between the brine and the rock surface which might alter the rock morphology. Then, we leave the brine for additional 48 h to settle and finally we filter it, using a fine filter paper, to remove the particles that might block the flow pathways of the rocks.

The density of brine is 1040.8 kg/m^3 measured using Anton Paar DMA 5000 M, and the viscosity is reported as 1.0085 mPa s (Lide 2004). The air/brine interfacial tension is 0.073 N/m measured using Ramé-Hart model 590 device, and the air viscosity is reported as 0.0018 mPa s (Tavassoli et al. 2005).

2.3 CT Imaging

We use one core of each rock type in this study. Table 1 shows the petrophysical properties of the rocks. We track the movement of the saturation front inside the rock by using a medical

Table 1 Summary of the petrophysical properties measured for the CT scanning co-current spontaneous imbibition experiment

Core label	Diameter (mm)	Length (mm)	ϕ (%)	k (m^2)	S_{gr}
E	37.7	76.5	27.6	2.10×10^{-13}	0.28
K	37.8	76.6	20.7	2.35×10^{-12}	0.28
P	37.9	76.4	22.1	5.23×10^{-15}	0.29

E, K, and P denote Estaillades, Ketton, and Portland, respectively

X-ray scanning instrument (HD-350E, Universal Systems). The purpose of the CT scanner is to identify the saturation profile and scale it to $\sqrt{t}$ to compare it with the analytical solution derived by Schmid et al. (2011) for spontaneous imbibition. We measure the weight of the core before and after we apply the heat shrink, when the core is completely dry. We apply the heat the shrink on the boundary of the core to make sure that co-current flow is applied.

We place the core vertically in the CT scanner domain, and we set the scanner operating parameters on a tube current of 225 mA and an energy level of radiation of 120 kV. Although flow is vertical, for the samples used the pressure difference due to buoyancy forces is much lower than the capillary pressure. After setting the scanner, we take a scan of the dry core and keep it as a reference which we will use to measure the saturation inside the core. Then we raise the brine reservoir until it touches the bottom surface of the core. After that, we take multiple scans at different times with one second acquisition time until the saturation front reaches the top of the core. Finally, we take a last scan when the saturation front reaches the top of the core and we use that as a reference scan. We measure the water saturation at each scan after the scan of the dry core and before the brine saturation reaches the top of the core by using

$$S_w = \frac{CT_{obj} - CT_{dry}}{CT_{brine} - CT_{dry}} \tag{38}$$

where S_w is the water saturation, CT_{obj} is the CT value of the processed image, CT_{dry} is the CT value of the dry image, and CT_{brine} is the CT value of fully saturated rock. We apply Eq. (38) to find the average saturation in slices perpendicular to the flow direction.

2.4 Capillary Pressure and Relative Permeability

In the Buckley–Leverett analysis for viscous-dominated flow, only relative permeability is needed to compute the analytical solution. For capillary-dominated flow, relative permeability and imbibition capillary pressure are needed to compute the analytical solution. In our theoretical analysis, we will assume Corey or power-law expressions for relative permeability and capillary pressure:

$$k_{rw} = k_{rw,max} \left(\frac{S_w - S_{wi}}{1 - S_{wir} - S_{gr}} \right)^n \tag{39}$$

where k_{rw} is the water relative permeability, $k_{rw,max}$ is the maximum water relative permeability, S_w is the water saturation, S_{wi} is the initial water saturation, S_{gr} is the residual gas saturation, and n is the Corey water exponent.

$$k_{rg} = k_{rg,max} \left(\frac{1 - S_w - S_{wi}}{1 - S_{wir} - S_{gr}} \right)^m \tag{40}$$

where k_{rg} is the gas relative permeability, $k_{rg,max}$ is the maximum gas relative permeability, S_w is the water saturation, S_{wi} is the initial water saturation, S_{gr} is the residual gas saturation, and m is the Corey gas exponent.

$$P_c = P_{c,entry}\left(\frac{S_w - S_{wi}}{1 - S_{wi} - S_{gr}}\right)^{\alpha} \tag{41}$$

where P_c is the capillary pressure, $P_{c,entry}$ is the entry capillary pressure, S_w is the water saturation, S_{wi} is the initial water saturation, S_{gr} is the residual gas saturation, and α is the capillary pressure exponent. We assume a strongly water-wet rock with complete displacement of movable gas by spontaneous imbibition: hence $S^* = 1 - S_{gr}$.

Then, we adjust the following parameters: $k_{rw,max}$, n, $k_{ro,max}$, m, $P_{c,entry}$, α so that the experimental results and analytical predictions match. However, this is not a unique determination of multiphase flow parameters since we have three functions—two relative permeabilities and a capillary pressure—to match one measured profile $S_w(\omega)$. We will explore this further in Discussion section.

3 Results and Discussion

3.1 CT Imaging Experiments and Comparison with Analytical Solutions

Figure 2 shows images of the water saturation profile obtained by CT scanning of each rock at different times. We can see that the water front of Estaillades has a hemispherical outwards shape, Portland's water front has a hemispherical inwards shape that merged to form a piston-like front at later times, while Ketton's water front has a piston-like displacement shape throughout the entire imbibition time. In a homogeneous medium, we would expect a uniform piston-like front. The variations from this that we observe may be due to heterogeneities in the core, or injection artifacts with either enhanced or suppressed flow at the side boundaries.

Figure 3 shows the slice averaged saturation profile of each rock at different times as a function of distance. The selected times cover a wide range of the water distance traveled for Estaillades and Ketton. However, for Portland, the times selected are after the water front merged into a piston-like profile. In Fig. 4, we show the averaged saturation profiles as a function of ω, Eq. (16). We can see that all the curves collapse approximately into one universal curve as a function of ω. Then, we compare the water saturation as a function of ω of each rock experimentally as well as analytically, as shown in Fig. 5.

The relative permeability and capillary pressure used in the analytic solutions were tuned to match the experimental results by varying the Corey and capillary pressure exponents by hand. We found that the water relative permeability and capillary pressure have the most impact on the analytical solution, while the air relative permeability had little influence on the results. This makes physical sense as the air has a low viscosity and is easily displaced: The movement of the water front is essentially entirely controlled by the water relative permeability (the ability to flow) and the capillary pressure (the driving force). Table 2 shows the input parameters used in the analytical solutions.

Our best match is when the k_{rw} exponent ≥ 8. Since the core is initially dry, the water relative permeability is low for low and intermediate water saturations, as water will first preferentially fill the largely disconnected microporosity, giving a large change in saturation but little increase in relative permeability, indicative of a high Corey exponent. The relative permeabilities and capillary pressures used for the matching are shown in Figs. 6 and 7,

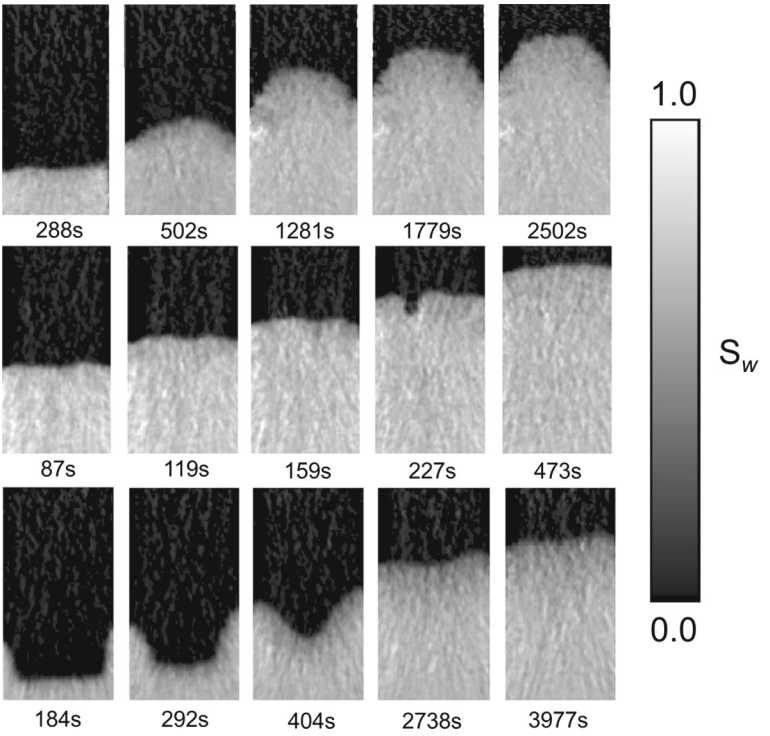

Fig. 2 CT cross section of air/brine spontaneous imbibition at different time intervals for (*top*) Estaillades, (*middle*) Ketton, and (*bottom*) Portland limestone rocks

respectively. The water saturation will have to increase to a large value in order to gain conductivity through the macroporosity (Fernø et al. 2013). The presence of initial water saturation is likely to provide conductivity and thus faster water fronts with smaller Corey exponents (Zhou et al. 2000; Li et al. 2002).

Several authors have estimated relative permeability and capillary pressure from spontaneous imbibition measurements (Li and Horne 2005; Haugen et al. 2014). In this study, we show that we can estimate the relative permeability and capillary pressure from matching the analytical solution with the experimental data. The solution is not unique since we have only one measured function and three saturation-dependent properties: two relative permeabilities and the imbibition capillary pressure. However, these experiments could be used in conjunction with traditional core flooding to determine all three functions together. Using conventional measurements of relative permeability (steady-state or using Buckley–Leverett theory in an unsteady-state experiment) and the spontaneous imbibition saturation profile, we can determine the imbibition capillary pressure. We could also determine the imbibition relative permeability from a measured capillary pressure and the spontaneous imbibition saturation profile. This is, however, a topic for future work, as we have not independently measured multiphase flow properties for these samples. As it stands, we can match the data but the functions used are not uniquely determined. Furthermore, this approach is only possible if we see $\sqrt{t}$ scaling of the imbibition front: A different method is needed if this is not the case.

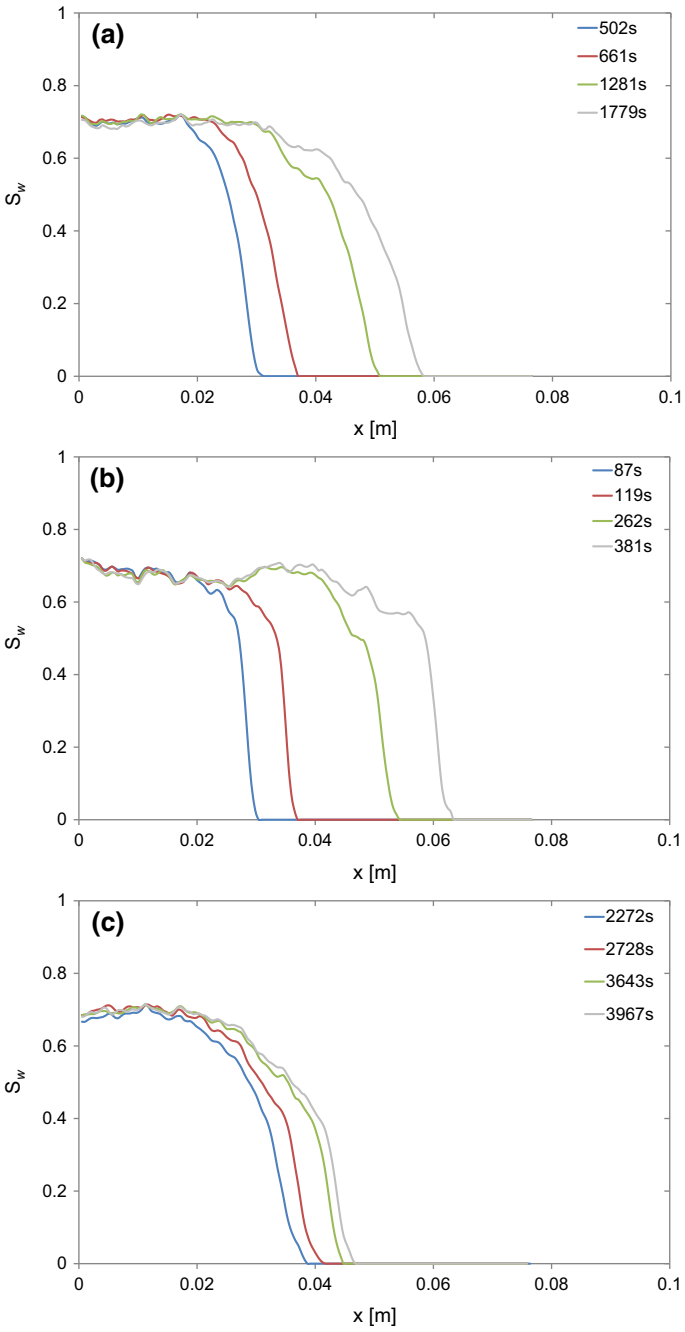

Fig. 3 Saturation profiles obtained from the CT acquisition as function of distance for **a** Estaillades, **b** Ketton, and **c** Portland

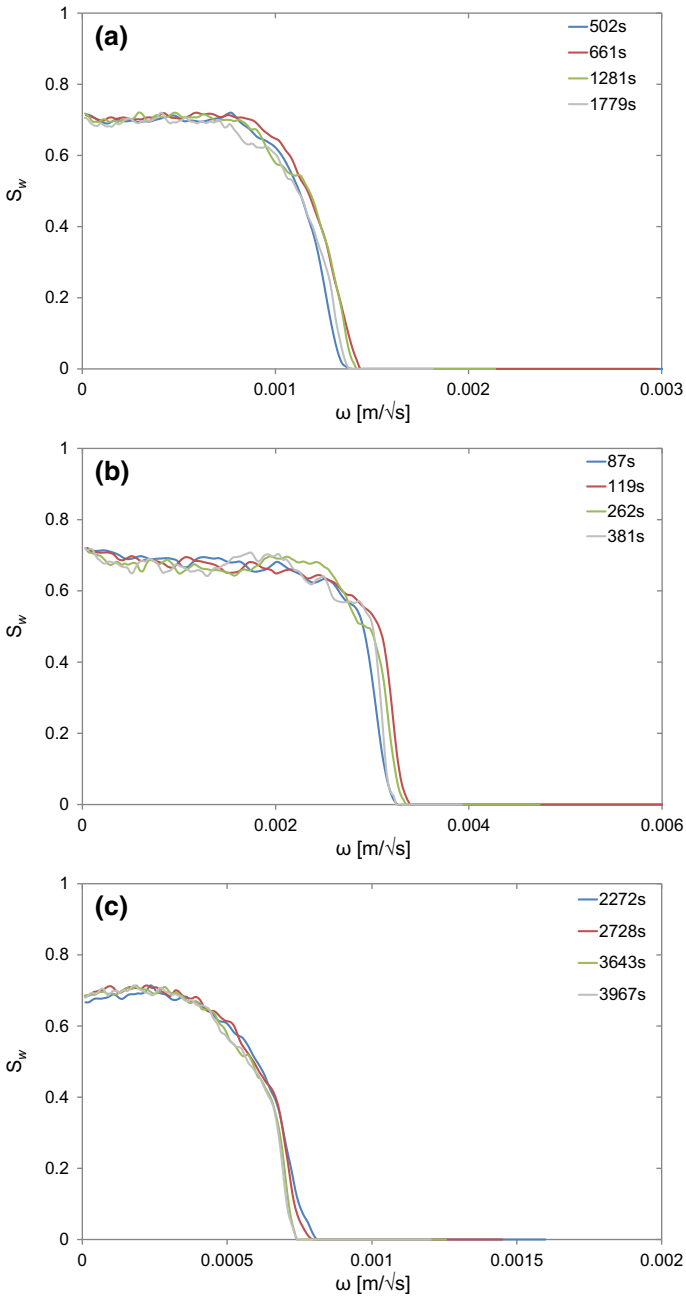

Fig. 4 Water saturation as a function of $\omega(x/\sqrt{t})$ after reprocessing Fig. 3 for **a** Estaillades, **b** Ketton, and **c** Portland

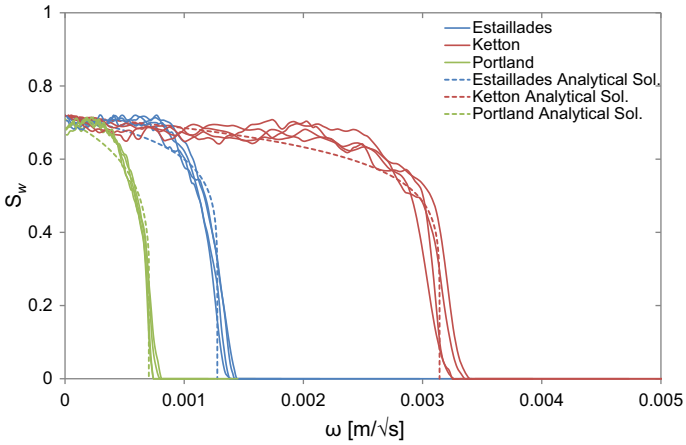

Fig. 5 Water saturation as a function of $\omega(x/\sqrt{t})$ for the three rocks comparing the experimental results with analytical solutions

Table 2 Input parameters used for the construction of the water saturation as a function of ω based on the analytical solution to match the experimental data

Input parameter	Estaillades	Ketton	Portland
S_{wi}	0	0	0
S_{gr}	0.28	0.28	0.29
n	10	10	8
$k_{\text{rw,max}}$	0.05	0.05	0.21
m	1.5	1.5	1.5
$k_{\text{rg,max}}$	0.8	0.8	0.8
$P_{\text{c,entry}}$ (Pa)	1,10,000	35,000	1,50,000
α	−1.5	−1.3	−1.3

3.2 Analytical Comparison of Co- and Counter-Current Imbibition

We are dealing with an air/brine fluid pair, with a very large viscosity ratio ($\mu_{\text{w}}/\mu_g \approx 56$). The difference between the co-current and counter-current analytical solution Eqs. (24) and (25), respectively, is the inclusion of the Buckley–Leverett fractional flow. In our system, this term will be close to 0 since we have a very high viscosity ratio. Figure 8 shows the Buckley–Leverett fractional flow along with the co-current and counter-current fractional flows based on the matched relative permeability and capillary pressure as shown in Figs. 6 and 7, respectively. We can see that the Buckley–Leverett fractional flow is close to 0 and therefore the co-current and counter-current fractional flows are close to each other. Figure 9 shows ω as a function of water saturation for both co-current and counter-current flow for the three rocks. The front for the co-current case is only slightly faster than the counter-current case, indicating that the behavior of co-current and counter-current is similar when dealing with an air/brine fluid pair. This difference is something that could be tested experimentally in future work, ideally with fluids of more similar viscosity, such as oil and water.

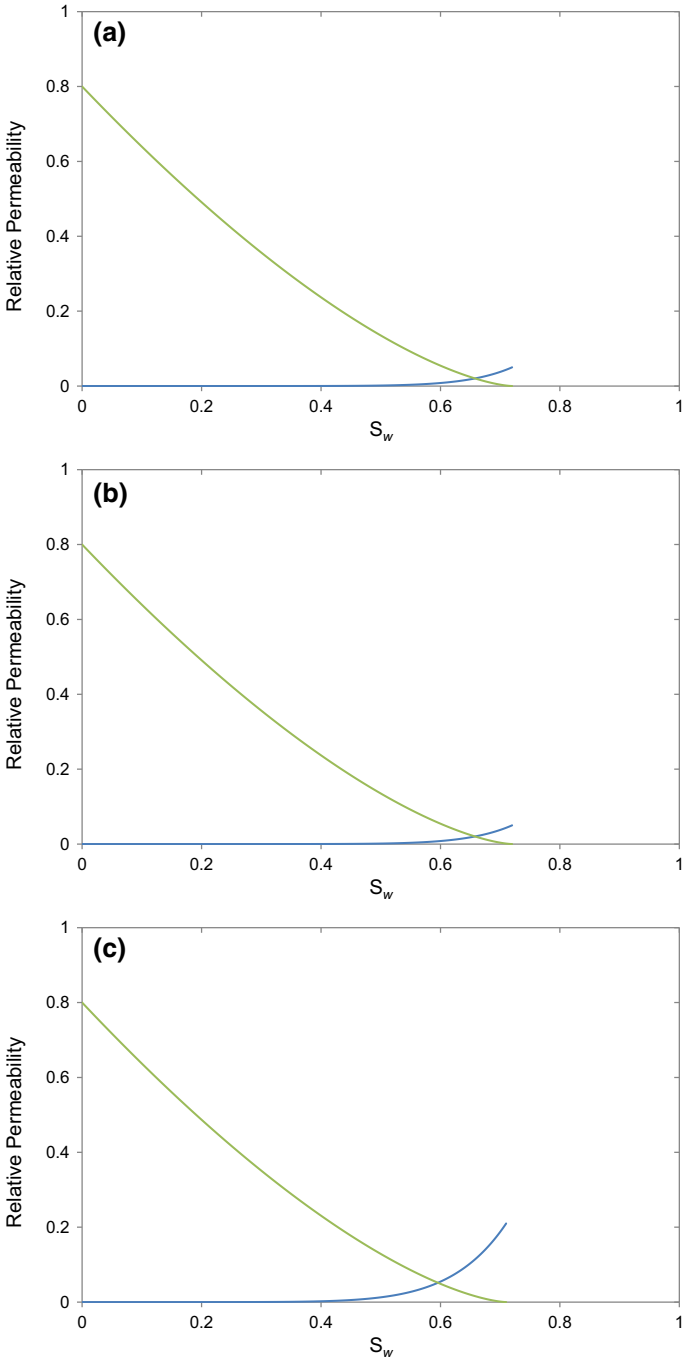

Fig. 6 Relative permeabilities used to match the analytical solution with the experimental data in Fig. 5 for **a** Estaillades, **b** Ketton, and **c** Portland. The *green curve* is the gas relative permeability, while the blue curve is the water relative permeability

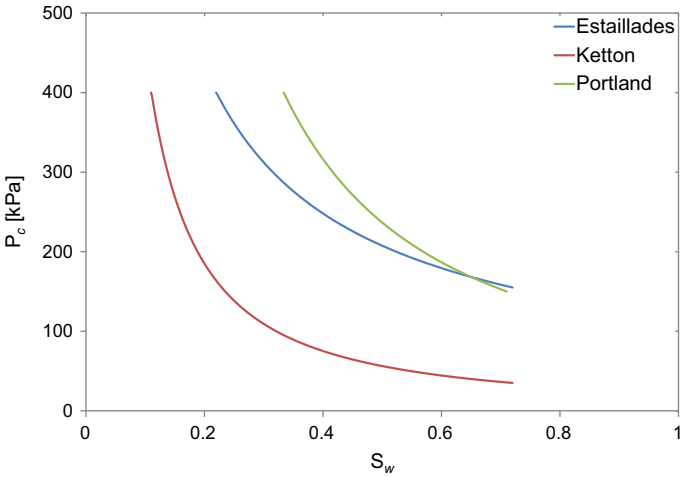

Fig. 7 Capillary pressures used to match the analytical solution with the experimental data in Fig. 5 for the three rocks

3.3 Use of the Analytical Solution

We will show how to use the analytical solution to estimate the relative permeability or capillary pressure from a spontaneous imbibition experiment. If we measure the saturation profile and we measure either the relative permeability using the steady or unsteady-state methods or capillary pressure using the centrifuge or the porous plate, then we can find the other parameter analytically. From a known profile $S_w(\omega)$ or $\omega(S_w)$, we can find F'' from Eq. (17) by differentiating the profile, while F is the integral, from Eq. (16):

$$F(S_w) = \int_{S_{wi}}^{S_w} \frac{\phi\omega(S_w)}{2C} \mathrm{d}S_w. \tag{42}$$

We can then use our determination of F and F'' in Eqs. (22) or (23) to determine $D(S_w)$, Eq. (14) directly. As an example, Fig. 10 shows $D(S_w)$ as a function of water saturation based on the analytical solution for the three rocks.

4 Conclusions

We have used the analytical solution for spontaneous imbibition derived by Schmid et al. (2011), to compare to spontaneous imbibition experiments where the average saturation profiles were measured using CT scanning. At early time, before the imbibing water front reaches the end of the core, the saturation profile is a function only of the distance divided by the square root of time. This form is a function of the imbibition relative permeabilities and capillary pressure. If we measure two of these three functions of saturation, then we could find the other function by matching to the analytical solution, providing a robust determination of multiphase flow properties.

Future work could extend this preliminary study to mixed-wet systems and to complement and constrain traditional core analysis measurements of relative permeability and capillary pressure.

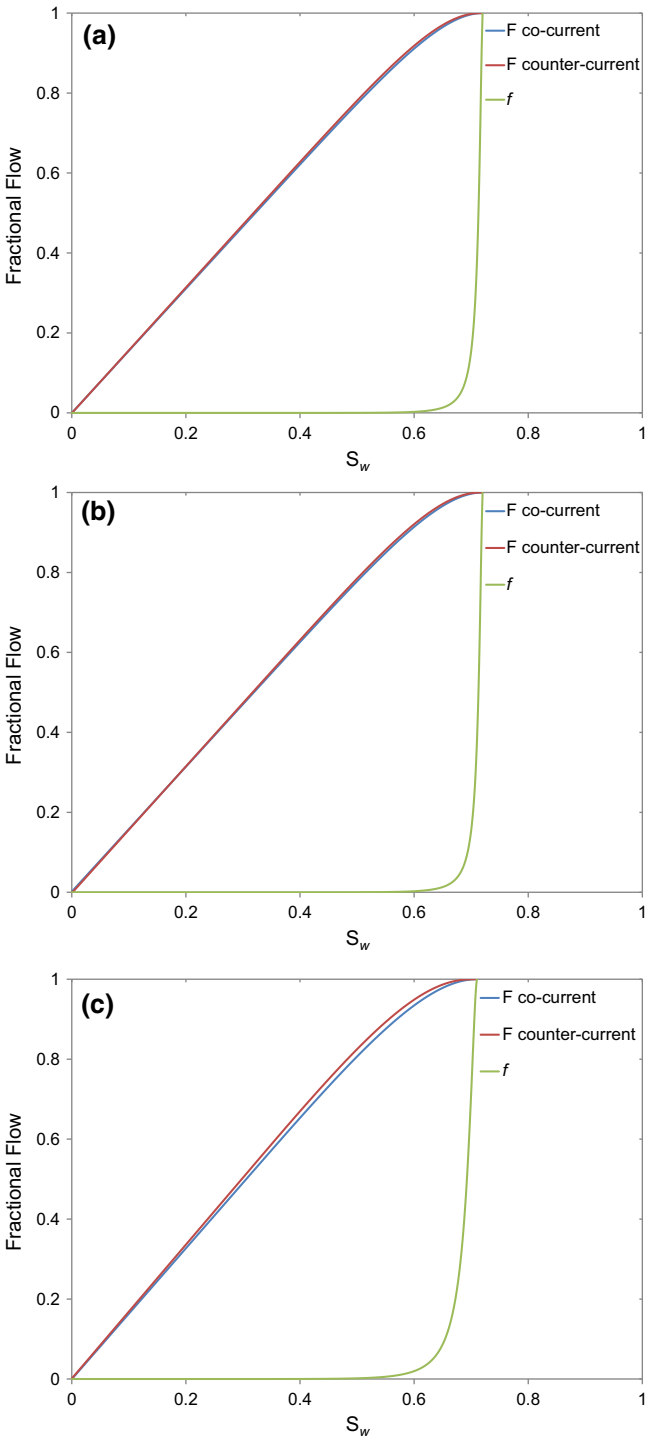

Fig. 8 Buckley–Leverett, co-current, and counter-current fractional flows for **a** Estaillades, **b** Ketton, and **c** Portland, based on the matched relative permeability and capillary pressure data

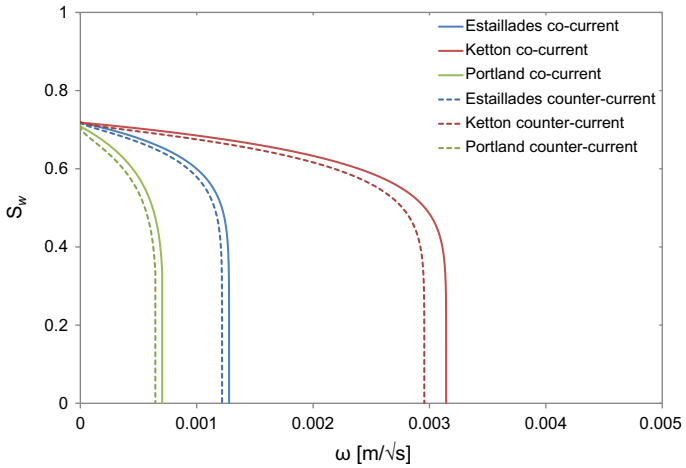

Fig. 9 ω as a function of water saturation comparing the behavior of co-current and counter-current flow based on the matched relative permeabilities and capillary pressures of the three rocks

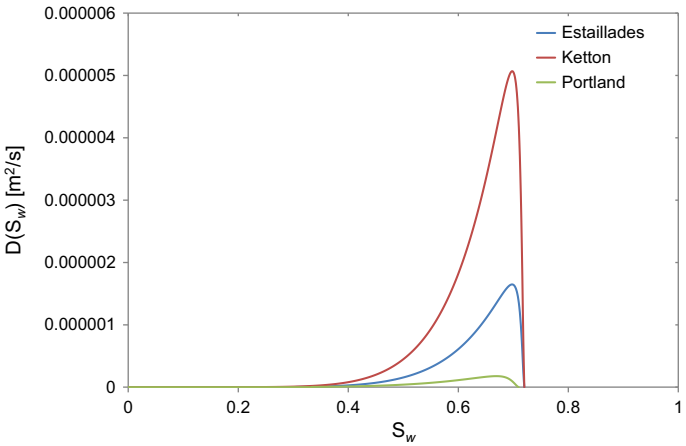

Fig. 10 Capillary dispersion coefficient, $D(S_w)$, as a function of water saturation for the three rocks

Acknowledgments We would like to acknowledge funding from the Qatar Carbonates and Carbon Storage Research Centre, QCCSRC, which is supported jointly by Qatar Petroleum, Shell and the Qatar Science & Technology Park.

References

Ashton, M.: The stratigraphy of the Lincolnshire limestone formation (Bajocian) in Lincolnshire and Rutland (Leicestershire). Proc. Geol. Assoc. **91**, 203–223 (1980)

Babadagli, B., Ershaghi, I.: Imbibition assisted two-phase flow in natural fractures. In: SPE Western Regional Meeting (1992)

Bourbiaux, B.J., Kalaydjian, F.J.: Experimental study of cocurrent and countercurrent flows in natural porous media. SPE Reserv. Eng. **5**, 361–368 (1990)

Brenchley, P.J., Rawson, P.F.: The Geology of England and Wales. The Geological Society, London (2006)

Buckley, S.E., Leverett, M.C.: Mechanism of fluid displacement in sands. Trans. AIME **146**, 107–116 (1942)
Dake, L.P.: Fundamentals of reservoir engineering, vol. 8. Elsevier, New York (1983)
Fernø, M.A., Haugen, Å., Wickramathilaka, S., Howard, J., Graue, A., Mason, G., Morrow, N.R.: Magnetic resonance imaging of the development of fronts during spontaneous imbibition. J. Pet. Sci. Eng. **101**, 1–11 (2013)
Garg, A., Zwahlen, E., Patzek, T.W.: Experimental and numerical studies of one-dimensional imbibition in Berea sandstone. In: American Geophysical Union Hydrology Days (1996)
Graue, A., Fernø, M.: Water mixing during spontaneous imbibition at different boundary and wettability conditions. J. Pet. Sci. Eng. **78**, 586–595 (2011)
Handy, L.L.: Determination of effective capillary pressures for porous media from imbibition data. AIME **219**, 75–80 (1960)
Haugen, Å., Fernø, M.A., Mason, G., Morrow, N.R.: Capillary pressure and relative permeability estimated from a single spontaneous imbibition test. J. Pet. Sci. Eng. **115**, 66–77 (2014)
Li, K., Horne, R.N.: Characterization of spontaneous water imbibition into gas-saturated rocks. SPE J. **6**, 375–384 (2001)
Li, K., Chow, K., Horne, R.N.: Effect of initial water saturation on spontaneous water imbibition. In: SPE Western Regional/AAPG Pacific Section Joint Meeting (2002)
Li, K., Horne, R.N.: Extracting capillary pressure and global mobility from spontaneous imbibition data in oil–water–rock systems. SPE J. **10**, 458–465 (2005)
Lide, D.R.: CRC handbook of chemistry and physics. CRC, Boca Raton (2004)
Mason, G., Fischer, H., Morrow, N.R., Johannesen, E., Haugen, Å., Graue, A., Fernø, M.A.: Oil production by spontaneous imbibition from sandstone and chalk cylindrical cores with two ends open. Energy Fuels **24**, 1164–1169 (2010)
Mason, G., Fernø, M.A., Haugen, Å., Morrow, N.R., Ruth, D.W.: Spontaneous counter-current imbibition outwards from a hemi-spherical depression. J. Pet. Sci. Eng. **90–91**, 131–138 (2012)
Mason, G., Morrow, N.R.: Developments in spontaneous imbibition and possibilities for future work. J. Pet. Sci. Eng. **110**, 268–293 (2013)
McWhorter, D.B., Sunada, D.K.: Exact integral solutions for two-phase flow. Water Resour. Res. **26**(3), 399–413 (1990)
McWhorter, D.B., Sunada, D.K.: Exact integral solutions for two-phase flow: reply. Water Resour. Res **25**(5), 1479 (1992)
Morrow, N.R., Mason, G.: Recovery of oil by spontaneous imbibition. Curr. Opin. Colloid Interf. Sci. **6**, 321–337 (2001)
Olafuyi, O.A., Cinar, Y., Knackstedt, M.A., Pinczewski, W.V.: Spontaneous imbibition in small cores. In: Asia Pacific Oil and Gas Conference (2007)
Pentland, C.H., El-Maghraby, R., Iglauer, S., Blunt, M.J.: Measurements of the capillary trapping of super-critical carbon dioxide in Berea sandstone. Geophys. Res. Lett. **38**, L06401 (2011)
Pooladi-Dravish, M., Firoozabadi, A.: Cocurrent and countercurrent imbibition in a water-wet matrix block. SPE J. **5**, 3–11 (2000)
Schmid, K.S., Geiger, S., Sorbie, K.S.: Semianalytical solutions for cocurrent and countercurrent imbibition and dispersion of solutes in immiscible two-phase flow. Water Resour. Res. **47**, W02550 (2011)
Schmid, K.S., Geiger, S.: Universal scaling of spontaneous imbibition for water-wet systems. Water Resour. Res. **48**, W03507 (2012)
Suzanne, K., Hamon, G., Billiotte, J., Trocme, V.: Experimental relationships between residual gas saturation and initial gas saturation in heterogeneous sandstone reservoirs. In: SPE Annual Technical Conference and Exhibition (2003)
Tavassoli, Z., Zimmerman, R.W., Blunt, M.J.: Analysis of counter-current imbibition with gravity in weakly water-wet systems. J. Pet. Sci. Eng. **48**, 94–104 (2005)
Unsal, E., Mason, G., Morrow, N.R., Ruth, D.W.: Co-current and counter-current imbibition in independent tubes of non-axisymmetric geometry. J. Colloid Interface Sci. **306**, 105–117 (2007)
Unsal, E., Mason, G., Morrow, N.R., Ruth, D.W.: Bubble snap-off and capillary-back pressure during counter-current spontaneous imbibition into model pores. Langmuir **25**, 3387–3395 (2009)
Wright, V.P., Platt, N.H., Marriott, S.B., Beck, V.H.: A classification of rhizogenic (root-formed) calcretes, with examples from the Upper Jurassic–Lower Cretaceous of Spain and Upper Cretaceous of southern France. Sediment. Geol. **100**, 143–158 (1995)
Zhang, X., Morrow, N.R., Ma, S.: Experimental verification of a modified scaling group for spontaneous imbibition. SPE Reserv. Eng. **11**, 280–285 (1996)
Zhou, X., Morrow, N.R., Ma, S.: Interrelationship of wettability, initial water saturation, aging time, and oil recovery by spontaneous imbibition and waterflooding. SPE J. **5**, 199–207 (2000)